Science of the Total Environment 814 (2022) 152654

Contents lists available at ScienceDirect

Science of the Total Environment

journal homepage: www.elsevier.com/locate/scitotenv

Impacts of biogenic emissions from urban landscapes on summer ozone and secondary organic aerosol formation in megacities

Yang Gao [a,*], Mingchen Ma [a], Feifan Yan [a], Hang Su [b,c], Shuxiao Wang [d], Hong Liao [e], Bin Zhao [d], Xuemei Wang [f], Yele Sun [g], James R. Hopkins [h], Qi Chen [i], Pingqing Fu [j], Alastair C. Lewis [h], Qionghui Qiu [d], Xiaohong Yao [a], Huiwang Gao [a]

[a] Frontiers Science Center for Deep Ocean Multispheres and Earth System, Key Laboratory of Marine Environment and Ecology, Ministry of Education, Ocean University of China, Qingdao National Laboratory for Marine Science and Technology, Qingdao 266100, China
[b] Max Planck Institute for Chemistry, Multiphase Chemistry Department, Mainz D-55128, Germany
[c] State Environmental Protection Key Laboratory of Formation and Prevention of Urban Air Pollution Complex, Shanghai Academy of Environmental Sciences, Shanghai 200233, China.
[d] State Key Joint Laboratory of Environment Simulation and Pollution Control, School of Environment, Tsinghua University, Beijing 100084, China
[e] Jiangsu Key Laboratory of Atmospheric Environment Monitoring and Pollution Control, Jiangsu Engineering Technology Research Center of Environmental Cleaning Materials, Collaborative Innovation Center of Atmospheric Environment and Equipment Technology, School of Environmental Science and Engineering, Nanjing University of Information Science & Technology, Nanjing 210044, China
[f] Guangdong-Hongkong-Macau Joint Laboratory of Collaborative Innovation for Environmental Quality, Institute for Environmental and Climate Research, Jinan University, Guangzhou 510000, China
[g] State Key Laboratory of Atmospheric Boundary Layer Physics and Atmospheric Chemistry, Institute of Atmospheric Physics, Chinese Academy of Sciences, Beijing 100029, China
[h] Wolfson Atmospheric Chemistry Laboratories, Department of Chemistry, University of York, York YO10 5NH, UK
[i] State Key Joint Laboratory of Environmental Simulation and Pollution Control, College of Environmental Sciences and Engineering, Peking University, Beijing 100084, China
[j] Institute of Surface-Earth System Science, Tianjin University, Tianjin 300072, China

HIGHLIGHTS

- Urban isoprene emissions improve the modeled isoprene concentration and diurnal cycle.
- Urban isoprene may trigger ozone formation twice as efficiently as that in rural area.
- The impact of biogenic emissions on secondary organic aerosol (SOA) is examined.

GRAPHICAL ABSTRACT

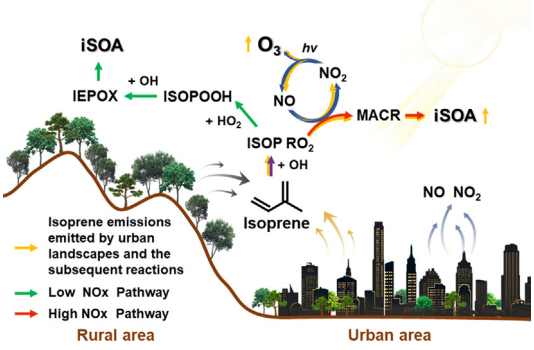

ARTICLE INFO

Article history:
Received 29 June 2021
Received in revised form 3 December 2021
Accepted 20 December 2021
Available online 29 December 2021

Editor: Pavlos Kassomenos

ABSTRACT

The impact of biogenic emissions on ozone and secondary organic aerosol (SOA) has been widely acknowledged; nevertheless, biogenic emissions emitted from urban landscapes have been largely ignored. We find that including urban isoprene in megacities like Beijing improves not only the modeled isoprene concentrations but also its diurnal cycle. Specifically, the mean bias of the simulated isoprene concentrations is reduced from 87% to 39% by adding urban isoprene emissions while keeping the diurnal cycle the same as that in non-urban or rural areas. Further adjusting the diurnal cycle of isoprene emissions to the urban profile steers the original early morning peak of the isoprene concentration to a double quasi-peak, i.e., bell shape, consistent with observations. The efficiency of ozone generation

* Corresponding author.
E-mail address: yanggao@ouc.edu.cn (Y. Gao).

http://dx.doi.org/10.1016/j.scitotenv.2021.152654

Keywords:
Biogenic emissions
Urban landscapes
Isoprene
Ozone
iSOA

caused by isoprene emissions in urban Beijing is found to be twice as large as those in rural areas, indicative of vital roles of urban BVOC emissions in modulating the ozone formation. Our study also shows that in the future along with NOx emission reduction, isoprene emissions from urban landscapes will become more important for the formation of ozone in urban area, and their contributions may exceed that of isoprene caused by transport from rural areas. Finally, the impact of biogenic emissions on SOA is examined, revealing that biogenic induced SOA accounts for 16% of the total SOA in urban Beijing. The effect of isoprene on SOA (iSOA) is modulated through two pathways associated with the abundance of NOx emissions, and the effect can be amplified in future when NOx emissions are reduced. The findings of our study are not limited to Beijing but also apply to other megacities or densely populated regions, suggesting an urgent need to construct an accurate emission inventory for urban landscapes and evaluate their impact on ozone and SOA in air quality planning and management.

1. Introduction

Biogenic volatile organic compound (BVOC) emissions are important precursors for the formation of ozone and secondary organic aerosol (SOA), and a number of studies have quantified their impacts on ozone (Derognat et al., 2003; Liu et al., 2019; Liu et al., 2018; Lu et al., 2019) and SOA (Hu et al., 2017; Qin et al., 2018).

The ozone pollution has recently become severe in China, particularly over the North China Plain (Li et al., 2019; Yan et al., 2021). While anthropogenic volatile organic compound (VOC) and NOx emissions play important roles in ozone formation, BVOCs are undoubtedly essential in constraining ozone formation and their role may be influenced by the changes of anthropogenic emissions. In a recent study focusing on ozone pollution period in June 2017 over urban Beijing (Gao et al., 2021), the synergic effect of biogenic and anthropogenic emissions has been thoroughly investigated, indicating that along the decrease of anthropogenic VOC or NOx emissions, the corresponding effect of biogenic emissions on ozone is characterized by a dipole pattern, concomitant with a linear enhanced or nonlinear weakened role, respectively. Moreover, the BVOCs emitted from different areas (e.g., urban or rural) may exert distinct effect on ozone. The BVOC emissions over urban areas are often co-located of NOx emissions, leading to more efficient ozone formation than that over rural areas (Bell and Ellis, 2004). In contrast, BVOCs that are not directly located in urban areas may only show moderate sensitivity for ozone enhancement under changes in NOx emissions, such as in the southeastern United States, because of location segregation between BVOCs (e.g., isoprene) and NOx (Travis et al., 2016).

BVOC emissions are primarily determined, under the influence of meteorology, by the plant functional types (PFTs), leaf area index, emission factors, among which PFTs may act as the key elements considering that the leaf area index and emission factors are tightly associated with PFTs (Guenther et al., 2012; Zhang et al., 2004). Recent studies have indicated that the widely used PFT data from the Moderate Resolution Imaging Spectroradiometer (MODIS) has a spatial resolution of 500-m, which is normally unable to resolve urban green spaces, thereby leading to missing of BVOC emissions from green spaces over urban areas when biogenic emission models, e.g., Model of Emissions of Gases and Aerosols from Nature (MEGAN;), are applied (Ma et al., 2019). Though in some regions like the United States, a higher spatial resolution of PFT data at 60-m (Guenther et al., 2012) is available in the community land model version 4 (CLM4), which may still only partly identify urban vegetation. In urban areas, it is common that a large number of trees are planted to help beautify the environment and act as air pollutant removers, alleviating global warming through carbon storage (McPherson et al., 2011; Morani et al., 2011). In turn, these trees may emit a sizable amount of BVOCs, triggering the enhancement of ozone and SOA.

Isoprene is considered one of the most abundant BVOC species. Specifically, the global total BVOC emissions from 2000 to 2012 were estimated to be 634 Tg C yr^{-1} from terrestrial vegetation, with isoprene accounting for 66% (Henrot et al., 2017). For ozone pollution, isoprene usually exhibits the largest ozone formation potential among multiple BVOC species (Ma et al., 2021; Zheng et al., 2009). Moreover, a recent study (Bryant et al., 2020) published observed isoprene concentration during the ozone pollution period (June 2017) in urban Beijing, motivating us to investigate the capability of the regional air quality model in reproducing the temporal variations and diurnal cycle of isoprene, as well as the synergic effect of anthropogenic emissions and isoprene emissions from urban green spaces or non-urban areas, which, to our knowledge, has not been well established so far.

In addition to ozone, BVOCs including isoprene and monoterpenes are believed to be dominant contributors to global SOA (Ehn et al., 2014; Farina et al., 2010). For instance, by carrying out measurements over 14 cities across different regions of China in summer 2012, Ding et al. (2014) found that for almost every city, the SOA formation from BVOCs accounted for more than two-thirds of the total SOA. The pathway by which isoprene yields SOA is strongly dependent on the amount of NO. For instance, under low NO conditions (Paulot et al., 2009), isoprene is first oxidized to isoprene hydroxyhydroperoxide (ISOPOOH) and then oxidized by OH to form isoprene epoxydiol (IEPOX); whereas under high NO conditions, through a series of reactions, isoprene can be oxidized to form hydroxymethyl-methyl-α-lactone (Nguyen et al., 2015) or 2-methyloxirane-2-carboxylic acid (methacrylic acid epoxide, MAE; Lin et al. (2013)). By comparing two biogenic emission inventories, Jiang et al. (2019) indicated that the one with higher monoterpene emissions may dramatically enhance SOA formation in Europe. However, little is known what role BVOCs from urban green spaces play in affecting urban SOA formation.

In what follows, we first evaluate how the applied model behaves in reproducing the magnitude and diurnal cycle of isoprene concentrations over urban Beijing. Followed by a comparison of ozone formation efficiency between isoprene emissions over urban areas and those from non-urban areas. Finally, the effect of isoprene and monoterpenes from urban landscapes on SOA is elucidated.

2. Method

2.1. Model configurations

The Weather Research and Forecasting (WRF) model (v 3.8.1) coupled with the Community Multiscale Air Quality (CMAQ) model (v 5.2) is applied to conduct the simulations. The simulation domain and period are the same as those in our previous studies (Gao et al., 2021; Yan et al., 2021) and mainly cover China and a few other countries in Asia at a spatial resolution of 36 km by 36 km from June 1 to July 5, 2017, with approximately one week prior to June 1 as spinup. The model configurations are similar to that in the previous studies (Gao et al., 2020; Ma et al., 2019; Yan et al., 2021). Briefly, physics options selected in WRF include the two-moment cloud microphysics scheme (Morrison et al., 2009), Rapid Radiative Transfer Model for GCMs (RRTMG) for both longwave and shortwave radiation parameterizations (Iacono et al., 2008; Morcrette et al., 2008), the unified Noah land surface model (Chen and Dudhia, 2001), the Mellor-Yamada-Janjic (MYJ) planetary boundary layer (PBL) scheme (Janjic, 1990; Janjic, 1994; Mellor and Yamada, 1982), and the Grell-Freitas cumulus parameterization scheme (Grell and Freitas, 2014). The gas chemistry and aerosol scheme used in CMAQ are carbon-bond version 6 (CB6) and Aerosol Module Version 6 (AERO6), respectively. The initial and boundary conditions of the WRF and CMAQ models are derived from the NCEP Climate Forecast System Reanalysis (CFSR) version 2 product (Saha et al., 2014) and Model for Ozone and Related chemical Tracers, version 4 (MOZART-4) product (Emmons et al., 2010), respectively.

The anthropogenic emissions are the same as those detailed in Ma et al. (2019) and Yan et al. (2021). In terms of biogenic emissions, standard simulations with MEGAN are first conducted. The land cover data used in MEGAN is the product of MODIS MCD12Q1 (Friedl et al., 2010) with the spatial resolution of 500-m, in general not being able to resolve the urban landscapes, indicating that only BVOC emissions over the non-urban areas across the entire simulation domain are included (referred to as NonUrban). Moreover, two scenarios are designed to add BVOCs emitted from urban green spaces over Beijing, in addition to those from non-urban area (NonUrban). The first scenario is to add 15% of the total BVOC emissions in Beijing to its urban core area spanning approximately 5000 km^2 (referred to as NonUrban + U-scaling), based on the vegetation survey in the previous study (Ren et al., 2017). Considering the broadleaf deciduous trees are the primary tree type in northern China (e.g., based on MODIS), the other scenario is to assign the land cover over urban Beijing the same as the selected grid over the non-urban area, after which the reallocated broadleaf deciduous trees over urban core account for approximately 15% of the total broadleaf deciduous trees in Beijing. After the relocation of PFT, MEGAN is conducted again to generate BVOC emissions, and this scenario is referred to as NonUrban + U-PFT. Please note BVOCs include more than 150 species, which are mapped to CB6 gas chemistry mechanism prior to the use in the air quality model CMAQ.

2.2. Information on observational data

The isoprene concentrations were measured hourly in June (till 24th) 2017 by a dual-channel GC with flame ionization detection (DC-GC-FID) at an altitude of approximately 102 m (39.97°N, 116.37°E) at the Institute of Atmospheric Physics (IAP), located in urban Beijing, China (Bryant et al., 2020). The concentrations of secondary inorganic aerosols including SO_4^{2-}, NO_3^- and NH_4^+, as well as organic aerosol (OA) were measured by high-resolution time-of-flight AMS (HR-ToF-AMS) at two sites. One site with a sampling altitude of about 4-m is located at IAP, the same location and measurement period as that for isoprene, and the other one is over the PKU Urban Atmosphere Environment Monitoring Station (PKUERS; 39.99°N, 116.31°E) approximately 8 km away from IAP, at a roof site approximately 30 m above the ground from June 1 to 14, 2017. The observation of SOA is available at IAP, calculated by the summation of more oxidized oxygenated OA (MO-OOA) and less oxidized oxygenated OA (LO-OOA) retrieved using the positive matrix factorization (PMF) method (Xu et al., 2019).

2.3. Experimental design

To investigate the impact of isoprene on ozone formation, as well as the synergic effect between anthropogenic NOx emissions (e.g., maintaining all the other anthropogenic emissions unchanged) and isoprene emissions on ozone, e.g., how isoprene modulates ozone concentration along with the reduction in NOx emissions, four sets of simulations are designed. Among different simulation sets (Table 1), anthropogenic NOx emissions are perturbed, from Base (without reduction) to maintaining NOx emissions over the entire domain at 80%, 50% and 20% of the level at Base, respectively, referred to as NOx0.8, NOx0.5 and NOx0.2. For each set of simulations (Table 1), three cases are designed with case ① excluding biogenic emissions, and the other two (cases ② and ③) either including isoprene emitted from non-urban areas (e.g., over the entire domain) or urban Beijing based on U-scaling method discussed in Section 2.1, and the comparison between cases ②, ③ and case ① can be used to isolate the effect of isoprene emissions from non-urban or urban areas on ozone in Beijing.

Table 1
Simulation sets designed to investigate the synergic effect between biogenic and anthropogenic emissions (Y and N indicate the corresponding emissions turned on and off, respectively).

Simulation sets	Anthropogenic NOx emissions	Isoprene emissions from non-urban area	Isoprene emissions from urban area	Cases
Base	100%	N	N	①
		Y	N	②
		N	Y	③
NOx0.8	80%	N	N	①
		Y	N	②
		N	Y	③
NOx0.5	50%	N	N	①
		Y	N	②
		N	Y	③
NOx0.2	20%	N	N	①
		Y	N	②
		N	Y	③

3. Results and discussions

3.1. Evaluation of the isoprene concentrations over urban Beijing

The simulated and observed isoprene concentrations over urban Beijing during June 2017 are compared and shown in Fig. 1. Despite of only one observational site available during the study period, the isoprene concentrations compiled from the previous studies (e.g., Fig. 7 in Ma et al. (2019)) exhibit comparable magnitudes across multiple sites in Beijing over a long-term period. Four scenarios of simulated results (Fig. 1a) are compared with observations (black), and the only differences lie in the source of BVOCs, including NonUrban (blue), NonUrban + U-scaling (green), NonUrban + U-PFT (orange) detailed in Section 2.1, as well as a fourth scenario which is the same as NonUrban + U-PFT except that the isoprene emissions over urban Beijing are doubled (referred to as Pseudo scenario; dashed red). By considering the BVOC emissions over non-urban areas (blue in Fig. 1a), an apparent underestimation of isoprene concentration is observed, with a mean bias of −0.45 ppbv (−87%). The simulations then show clearly discernable improvement and the mean bias is reduced to 39% by adding isoprene emissions from urban Beijing based on the U-scaling method (green in Fig. 1a).

In addition to reducing the mean bias, the diurnal cycle of isoprene is improved as well. The observations show a peak in the morning at approximately 9:00 am and fluctuate until late afternoon, leading to a second quasi-peak at approximately 14:00 (black lines in Fig. 1b,c). The early morning peak is understandable as the time when isoprene emissions are relatively strong but photochemical reactions are weak, yielding an accumulation and enhancement of isoprene concentration. Along with intensification of photochemical reactions in the daytime, the isoprene concentrations decrease due to high chemical reactivity with the primary sink of OH, and relatively short lifetime (e.g., 20-min from 10:00–15:00 during the study period; Bryant et al. (2020)). While the scenario of NonUrban tends to amplify the second peak in the late afternoon, an early morning peak of the isoprene concentrations is nicely captured by the scenario of NonUrban + U-scaling, either from June 1 to July 5, 2017 or during the ozone episodic event from June 14 to 21 (green vs. blue in Fig. 1b,c). Nevertheless, the simulated isoprene concentrations in this scenario somewhat monotonically decrease after 9:00 am (green in Fig. 1b,c), with the possible mechanism discussed below.

Given that the isoprene emissions from urban landscapes in the U-scaling method are directly scaled by 15% from that over the non-urban areas of Beijing, the temporal profiles of isoprene emissions between non-urban and urban areas are therefore the same. Biogenic emissions are highly correlated with temperature and light (Mayrhofer et al., 2005), and the most closely associated meteorological parameters include photosynthetically active radiation (PAR), near surface water vapor (Q2) and air temperature at 2 m (TEMP2). The diurnal cycles of these parameters simulated from WRF over urban and non-urban areas (Fig. S1) exhibit obvious differences between urban and non-urban areas. For instance, the temperature tends to be higher over urban areas with less water vapor content, indicating hotter and drier conditions, which are more prone to stimulate biogenic emissions (Calfapietra et al., 2013). This contrast in meteorological conditions between urban and non-urban areas, as well as

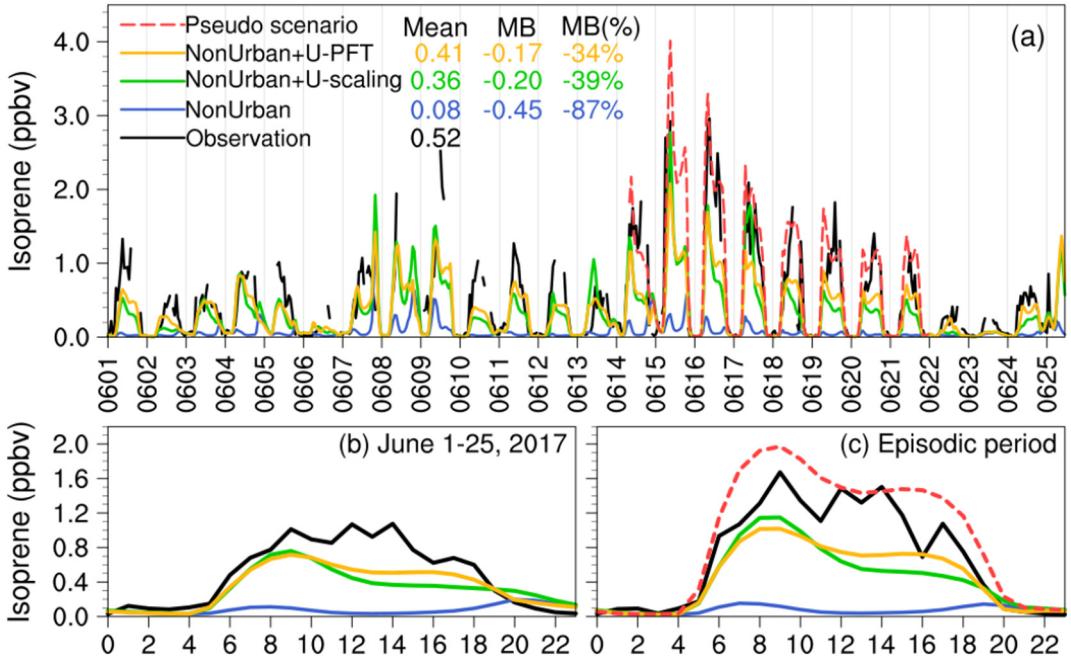

Fig. 1. Time series of isoprene concentrations between observations (39.97°N, 116.37°E) and the simulations over the corresponding grid in urban Beijing during June 1–25, 2017 and ozone episode during June 14–21, 2017. The black line represents the value from observational data, the other lines represent the simulated isoprene concentrations based on four scenarios, including NonUrban (blue), NonUrban + U-scaling (green), NonUrban + U-PFT (orange) and Pseudo scenario (dashed red; Fig. 1a, c). (For interpretation of the references to colour in this figure legend, the reader is referred to the web version of this article.)

the PBL differences, e.g., relatively higher PBL in urban areas compared to non-urban areas during the same period, is consistent with the findings in Tao et al. (2022), which included the anthropogenic heat in and around Beijing. Meanwhile, the peak radiation in urban areas is approximately 1–2 h later than that over non-urban areas (second row in Fig. S1), which is consistent with the downward incoming shortwave radiation from the same simulation results.

To delve into the influences on isoprene emissions and concentrations caused by differences in the diurnal cycle in meteorological conditions between urban and non-urban areas, the scenario of NonUrban + U-PFT is conducted (detailed in Section 2.1). The resulting diurnal cycle of isoprene emissions over urban areas implies a peak at approximately 14:00 (orange in Fig. S2), which is 1–2 h later than that in the NonUrban + U-scaling scenario (green in Fig. S2). The time series and diurnal cycle of isoprene concentration simulated from CMAQ for the NonUrban + U-PFT scenario are shown in orange in Fig. 1a-c. Although the magnitude of the isoprene concentration is generally comparable to that in NonUrban + U-scaling scenario, the temporal distribution becomes more reasonable; thus, instead of monotonically decreasing after 9:00 am, the trend becomes much smoother with a slight increase after noon, although an exact match is not achieved. The simulated hourly ozone concentration enhancement averaged over urban Beijing, due to changes in the diurnal cycle of isoprene emissions under the NonUrban + U-PFT scenario relative to NonUrban + U-scaling, may reach as high as 3.57 ppbv.

Considering the underestimates of isoprene concentration in either NonUrban + U-scaling or NonUrban + U-PFT scenario particularly during the episodic event (green and orange vs. black in Fig. 1c), a pseudo scenario is designed through artificially boosting the isoprene emissions over urban Beijing by 100% relative to the U-PFT scenario, aiming to evaluate the sensitivity of isoprene concentrations to changes in isoprene emission amounts. The resulting isoprene concentrations are considerably close to the observations (dashed red in Fig. 1a,c), indicating likely underestimates of broadleaf deciduous trees based on the current method. Moreover, the bias may be attributed to a few other factors, i.e., relatively low spatial resolution of the simulations, with a higher resolution preferred to better resolve the spatial heterogeneity in megacities, particularly over the areas surrounded by green spaces or forest parks, or the inaccuracy in the isoprene emissions estimation based on the current method. In the analysis below, whenever biogenic emissions over urban Beijing are used, the method of U-scaling is applied, and the scenario such as U-PFT should yield comparable results.

3.2. Impact of isoprene emissions from urban and non-urban areas on ozone concentrations over urban Beijing

In urban areas, BVOC emissions may play important roles in ozone formation since urban areas are prone to be VOCs-limited; therefore, the previously missed biogenic emissions from urban landscapes may play key roles in affecting the ozone concentrations therein. Considering that isoprene exhibits the largest ozone formation potential among BVOCs (Ma et al., 2021), instead of using all BVOCs, only isoprene emissions are added besides anthropogenic emissions, aiming to elucidate the effect of isoprene emissions over urban or non-urban areas on ozone formation in urban Beijing.

As reported by Travis et al. (2016), when the spatial distribution of isoprene and NOx emissions were segregated, isoprene may only be moderately sensitive to changes in NOx emissions. It is thus of great interest to elucidate the evolution of ozone under changes in anthropogenic NOx emissions when they are collocated with isoprene emissions from urban green spaces. Considering that daytime from 9:00–16:00 is concomitant with strong photochemical reactions (e.g., Yan et al. (2021)), the following analysis focused only on this time window based on the simulations listed in Table 1. From June 1–July 5, the monthly mean contribution to daytime ozone is 2.48 ppbv and 4.76 ppbv, respectively, from isoprene over urban and non-urban areas at Base case (leftmost bar in Fig. 2a), with the contribution from urban isoprene emissions accounting for approximately one-third of the total isoprene emissions.

Along with the reduction in NOx emissions (second to fourth groups of bars in Fig. 2a), the overall contribution from biogenic isoprene emissions to ozone become smaller relative to Base (first bar in Fig. 2a), consistent with the previous finding (e.g., Fig. 4b,d in Gao et al., 2021). Nevertheless, the contributions of urban isoprene emissions on ozone formation becomes higher relative to those from non-urban area. For instance, over urban Beijing, the mean contribution to ozone from isoprene emissions due to

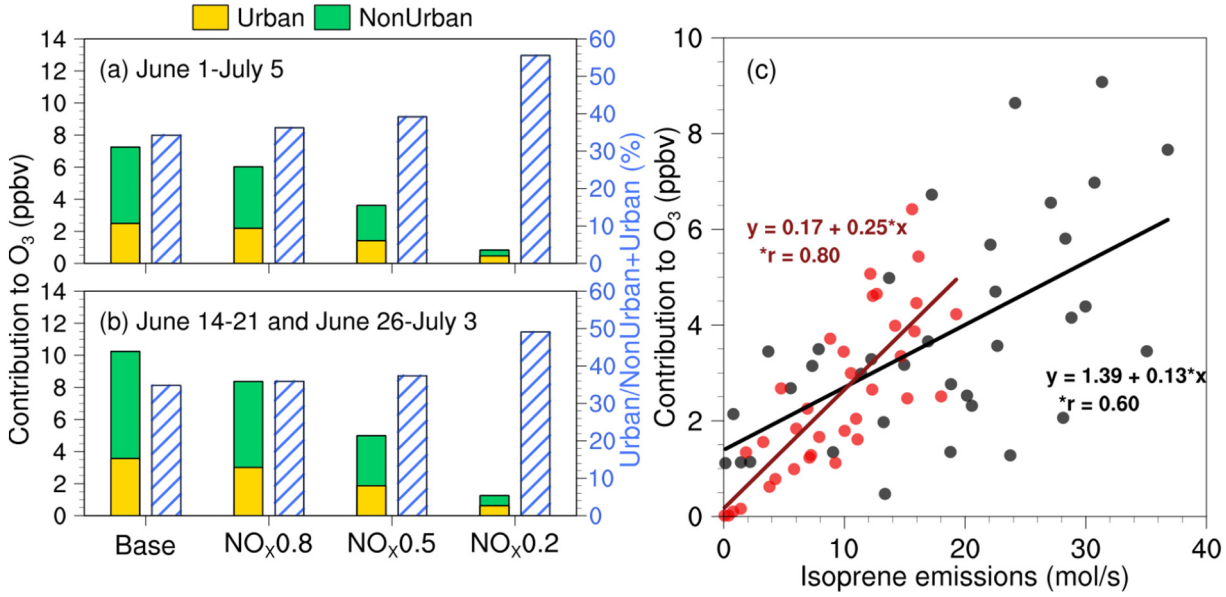

Fig. 2. Left: Contribution to ozone over urban Beijing due to isoprene from urban green spaces (Urban; orange) and non-urban area (NonUrban; green) for Base, and cases with NOx reductions of 20% (NOx0.8), 50% (NOx0.5) and 80% (NOx0.2) from June 1–July 5 (Fig. 2a), June 14–21 and June 26–July 3, respectively (Fig. 2b), with the percentage contribution from urban shown by the hatched line, which corresponds to the Y axis on the right. **Right:** Mean ozone contribution during June 1–July 5 from isoprene emissions averaged over urban (red) and rural (black) areas (Fig. 2c). Only the daytime 9:00–16:00 LST is used in the analysis. (For interpretation of the references to colour in this figure legend, the reader is referred to the web version of this article.)

urban landscape increases as NOx is reduced and accounts for 36%, 39% and 56% when NOx emission reductions reach 20% (NOx0.8), 50% (NOx0.5) and 80% (NOx0.2), respectively. A similar phenomenon is found during the ozone episodes (June 14–21; June 26–July 3; Fig. 2b). The monotonic increase in percentage contribution to ozone from urban isoprene emissions (hatched bars in Fig. 2a,b), along with NOx emission decreases, implies a higher efficiency of isoprene emitted from urban green spaces relative to that transported from non-urban areas particularly when NOx emissions gradually become insufficient, indicating an enhanced ozone accumulation effect resulting from the colocation between NOx and isoprene emissions.

To delve into the efficiency of isoprene emissions on the enhancement of ozone formation, a scatter plot of hourly isoprene emissions from urban and non-urban area and the corresponding ozone concentrations, simulated in Base case, is shown in Fig. 2c. The results indicate that the efficiency of ozone formation caused by isoprene emissions from urban landscapes (slope of 0.25) is almost twice as high as that over non-urban areas (slope of 0.13). It is noteworthy that the case including isoprene emissions from the non-urban areas (Table 1) take into account the isoprene emissions in both Beijing and the other regions in the simulation domain, whereas the other case with isoprene emissions from urban landscapes solely include those in urban Beijing. From this perspective, the comparison constructed in this study may lie in the lower limit of the effect of isoprene from urban green spaces on ozone, implicative of a potentially more important role of urban isoprene emissions on ozone formation in megacities.

In addition to isoprene emissions, it is useful to elucidate the contributions of all the other BVOCs, from urban green spaces or non-urban areas, on ozone concentrations as a comparison. To this end, another four sets of numerical simulations are conducted identical to those shown in Table 1, except the isoprene replaced by other BVOCs (Fig. S3). The contribution of BVOC emissions (without including isoprene) from urban green spaces to ozone in urban Beijing are in general less than 20%, much smaller than those from the non-urban area (orange vs. green bars in Fig. S3), and the contributions are comparable to and even slightly larger than those from isoprene emitted over non-urban areas (green bars; Fig. S3 vs. Fig. 2), partly attributable to longer lifetime of the other BVOCs relative to isoprene and subsequently yielding larger effect from the transport. Along the reduction of anthropogenic NOx emissions, the effect of the other BVOCs from urban landscapes, relative to those from non-urban areas, on ozone concentration over urban Beijing maintains similar increasing tendency as those from the isoprene emissions except of a much smaller effect when NOx emissions reduce to 20% (hatched bars in Fig. 2 vs. Fig. S3).

Instead of perturbing BVOCs, four more simulation sets are conducted along the reduction of NOx emissions displayed in Table 1, and for each set, while keeping isoprene emissions from both the urban and non-urban areas the same, it includes a pair of simulations with and without anthropogenic VOC emissions over the simulation domain. The differences between the paired simulations over each set is considered the contributions of anthropogenic VOC emissions on ozone concentrations in urban Beijing (Fig. S4). The results reveal decreasing impacts of anthropogenic VOCs on ozone along NOx emission reductions, consistently with that of biogenic emissions (Fig. 2 vs. Fig. S4), despite of a much larger effect from anthropogenic VOC emissions primarily caused by the higher amount. It is worth to mention that this effect has been detailed in the previous study (e.g., Fig. 2a in Gao et al., 2021), and the clear NO titration effect indicated therein tends to become weaker in this study, presumably a result of the time window of daytime applied in this study, when the strong photochemical reactions partly subdue the emergence of titration effect.

The incremental ozone concentrations because of biogenic emissions from urban green spaces may affect a wider area due to transport, however, it is not clear to what extent the influence may invade spatially. To address this question, four time periods dominated by different wind patterns are selected, as shown in Fig. 3. As an illustration, spatial distributions of ozone concentrations shown in Fig. 3a-d reflect the effect of isoprene emissions from urban landscapes only (differences between the case ① and ③ in the Base simulation set in Table 1), and the impact could be transported to a few hundred kilometers away from the source region. The transport pathways of ozone are consistent with the trajectory from WRF- FLEXible PARTicle dispersion model (FLEXPART) (Fig. 3e), yielding a maximal influence at 3.49 ppbv outside urban Beijing based on the temporal average of each period.

3.3. Impact of biogenic emissions on SOA over urban Beijing

In addition to ozone, we evaluate the capability of CMAQ in reproducing observed secondary inorganic aerosols (including SO_4^{2-}, NO_3^-, NH_4^+),

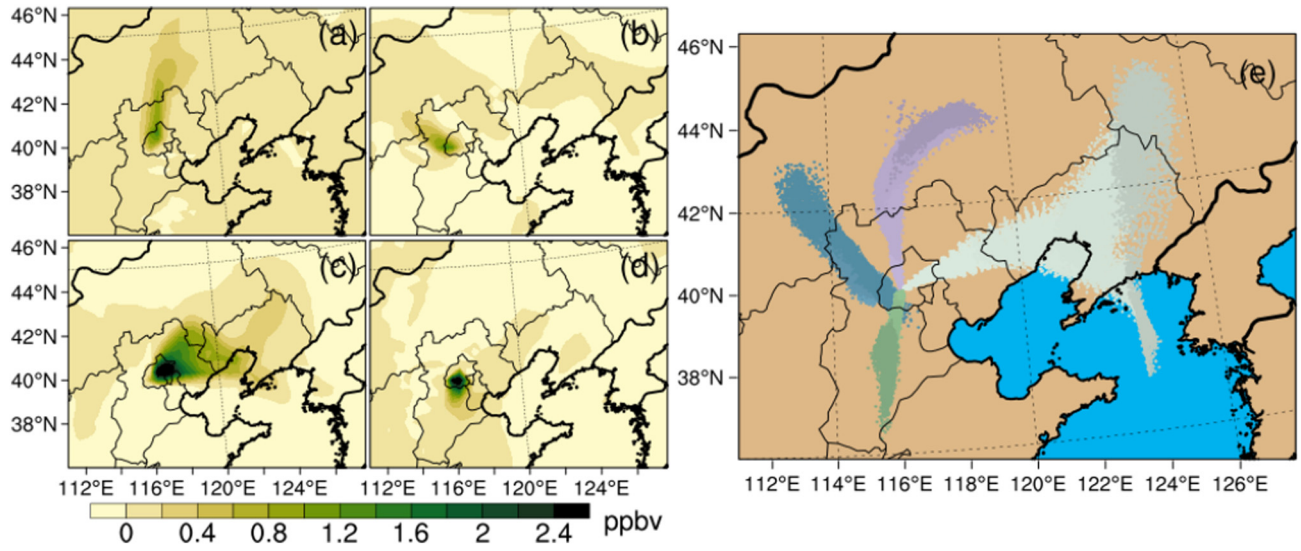

Fig. 3. Left: Spatial distribution of ozone concentrations due to influence of isoprene emissions from green spaces, during the time (local standard time; LST) from 12:00 pm June 5 to 6:00 am June 6 (Fig. 3a), 10:00 am June 12 to 2:00 am June 13 (Fig. 3b), 11:00 am June 15 to 8:00 pm June16 (Fig. 3c), 8:00 am to 8:00 pm on June 25 (Fig. 3d). **Right:** Trajectories from WRF-FLEXPART, with different colors (purple: northward, deep skyblue: northwestward, gray: northeastward and green: southward) corresponding to the time periods in Fig. 3a-d. (For interpretation of the references to colour in this figure legend, the reader is referred to the web version of this article.)

total OA, and SOA during the same period from June 1 to 25 as that for isoprene, as shown in Fig. 4. The observational data from both sites (PKU and IAP) are quite comparable, warranting the robustness of the sites in representing the air pollutant concentrations over the urban Beijing. The model exhibits a skillful ability in simulating secondary inorganic aerosols (Fig. 4a-c). While OA is strongly underestimated (Fig. 4d), the SOA is

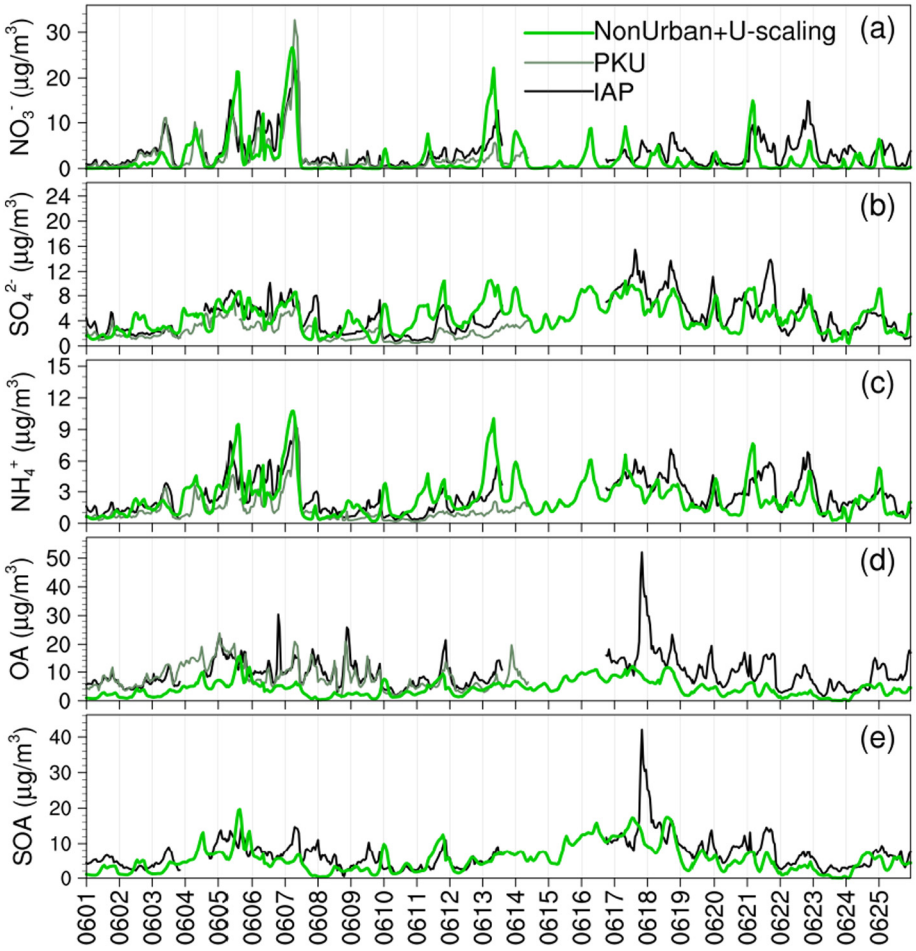

Fig. 4. Evaluation of NO_3^-, SO_4^{2-}, NH_4^+, organic aerosol (OA) and secondary organic aerosol (SOA) over urban Beijing. The observations over two sites (described in Section 2.2) of PKU and IAP are used. Please note that the observation of SOA is only available at IAP.

much better reproduced by the model despite the slight underestimation of 1.91 μg/m^3 (Fig. 4e), implying that the underestimates of OA is highly associated with the primary OA. The observational mean SOA from June 1 to 25 is 6.86 μg/m^3, which is slightly larger than that reported by Ding et al. (2014) in urban Beijing during summer 2012, ranging from 2.33 μg/m^3 to 8.17 μg/m^3 with a mean value of 4.15 μg/m^3. Moreover, an evaluation of $PM_{2.5}$ (not shown) during the same period indicates a mean fractional bias (MFB) and error (MFE) at −47% and 54%, respectively, in general satisfying the benchmarks (MFB/MFE: 50%/75%) proposed by the US EPA (USEPA, 2007).

To investigate the impact of BVOC emissions on the SOA, the time series of simulated biogenic SOA (BSOA) and total SOA over urban Beijing from June 1 to July 5 is shown in Fig. 5a. The mean concentrations of BSOA and SOA during the simulation period are 1.15 μg/m^3 and 7.16 μg/m^3, respectively, with BSOA accounting for 16%. The peak SOA concentrations occur concomitantly with high temperatures, i.e., the end of June and early July. The enhancement effect of temperature on BSOA seems to be more efficient than that on SOA, particularly over the early stage of the high-temperature period; thus, temperature could potentially yield a much higher percentage contribution of BSOA to total SOA at that time. For instance, the contribution increases from 23% on June 24 to 43% and 50% on June 25 and 26, respectively (dashed gray in Fig. 5a), when temperatures become higher on the latter days (e.g., dashed blue in Fig. 4d in Ma et al., 2019).

To address the influence of isoprene on SOA (iSOA) formation over urban Beijing, two scenarios of NonUrban and NonUrban + U-scaling (detailed in Section 2.1) are used in the comparison. The total iSOA concentrations without counting urban BVOC emissions (red in Fig. 5b) range from 0.08 μg/m^3 to 1.68 μg/m^3, with a mean value of 0.63 μg/m^3, and the incremental effect of isoprene from the urban landscapes to iSOA is 8% (red vs. green in Fig. 5b). The magnitude of iSOA is comparable to the observations displayed in Fig. 9b in Bryant et al. (2020), while it is lower than that reported by Ding et al. (2014) with a mean value of 1.59 μg/m^3 during July–September 2012, which is partly attributable to the sample collection frequency of once every two weeks with a duration of 48 h therein. Meanwhile, the time series of SOA depicted from the observation (black in Fig. 4e) clearly implies that fluctuations of the temporal profile is not trivial; thus, a biweekly sample may yield a large difference compared to the mean value of more frequent sampling (e.g., hourly resolution in this study). In addition, the mean contribution of monoterpenes

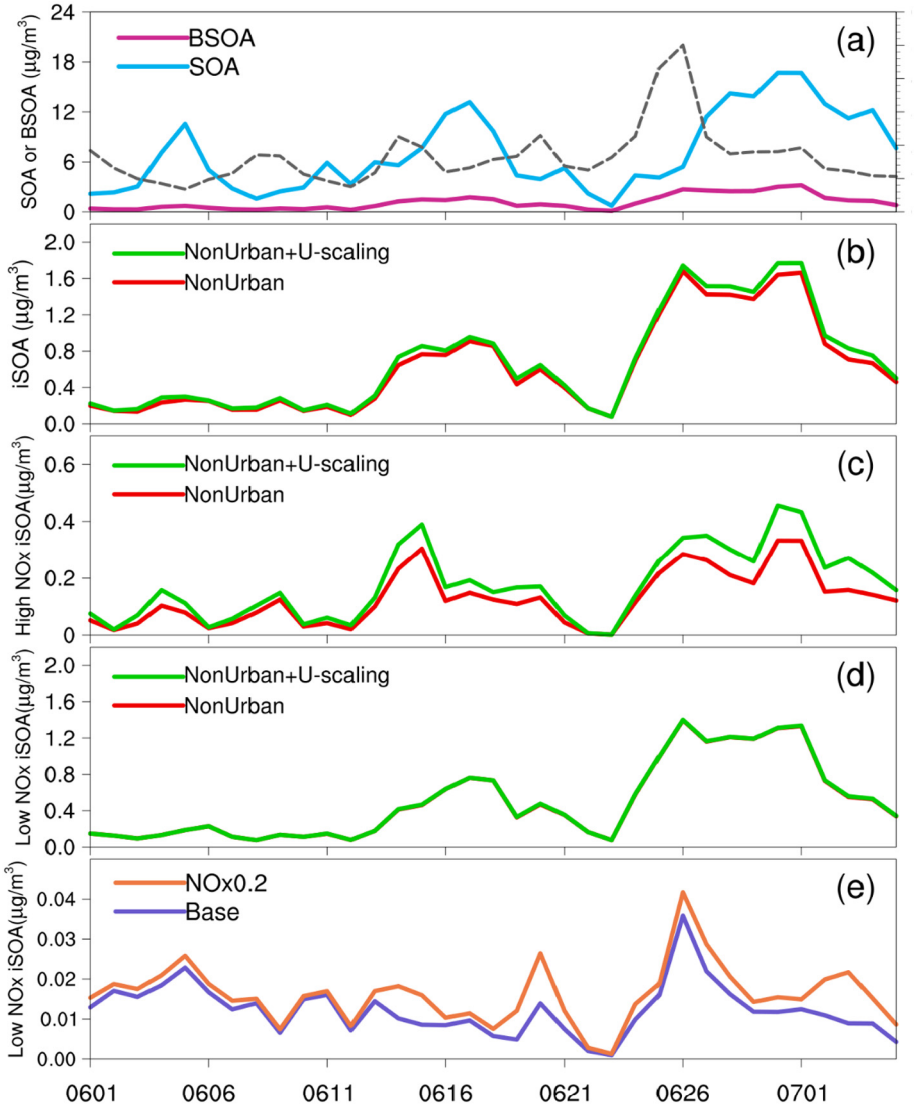

Fig. 5. Time series of SOA or BSOA (Fig. 5a) under the scenario of NonUrban + U-scaling, total iSOA (Fig. 5b), high NOx iSOA (Fig. 5c) and low NOx iSOA (Fig. 5d) under scenarios of NonUrban + U-scaling (green) and NonUrban (red), over urban Beijing. The bottom panel (Fig. 5e) shows low NOx iSOA over urban Beijing in two cases (case ③ for the simulation set of Base and NOx0.2 in Table 1). (For interpretation of the references to colour in this figure legend, the reader is referred to the web version of this article.)

to SOA is 0.16 μg/m^3 (green in Fig. S5), with those from urban green spaces contributing to 25%. Nevertheless, the contribution from monoterpenes is less than a quarter of that from isoprene (0.68 μg/m^3) to SOA in urban Beijing (green; Fig. S5 vs. Fig. 5b), likely associated with the smaller amount of terpenes in comparison to isoprene emissions therein (e.g., Supplementary Table 6 in Ma et al., 2021).

As mentioned in the introduction, there are two major pathways by which isoprene yields SOA dependent on the availability of NO; therefore, the total iSOA (Fig. 5b) can be classified into high NOx iSOA and low NOx iSOA (Fig. 5c,d). Without considering BVOC emissions from the urban landscapes, the mean iSOA from the high NOx pathway is 0.13 μg/m^3 (red in Fig. 5c), and an increase of 36% is achieved by adding urban BVOC emissions (green in Fig. 5c). The iSOA from the low NOx pathway is on average 0.50 μg/m^3 (red in Fig. 5d), which is a few times higher than that from the high NOx pathway, and a sizable portion is transported from the non-urban area, with little change in low NOx iSOA found by the inclusion of BVOC emissions from urban landscapes (red vs. green in Fig. 5d).

Considering that urban areas normally have an abundance of NOx and the emissions of NOx may decrease substantially in the future, the simulation results based on the two cases (case ③ for the simulation set of Base and NOx0.2 in Table 1) are used to elucidate how changes in NOx emissions will modulate the low NOx iSOA (Fig. 5e). The mean iSOA in urban Beijing contributed solely from urban isoprene is only 0.012 μg/m^3, which is much smaller than that (e.g., NonUrban) displayed in Fig. 5d, likely caused by the wider area with abundant isoprene emissions in non-urban Beijing, under which high iSOA is formed and transported to the urban area. When NOx is reduced by 80% (NOx0.2), the iSOA concentrations due to urban isoprene increase by 31%, with a maximal hourly enhancement at 0.11 μg/m^3, which indicates a positive role of NOx reduction in elevating the iSOA formed under the low NOx pathway. Compared with ozone, for which isoprene emissions over urban areas show strikingly higher efficiency than those over non-urban areas, iSOA is more likely to be formed in non-urban areas since the low NOx pathway tends to be dominant. Nevertheless, the effect of urban isoprene does play a nonnegligible role, and it becomes even larger under the decrease in NOx emissions. The mechanisms for ozone as well as SOA enhancement due to isoprene emissions from urban landscapes are summarized in Fig. 6.

4. Conclusions

By taking into account the previously missed isoprene emissions from the urban landscapes in Beijing, we thoroughly investigate their potential influences on the isoprene, ozone and SOA concentrations. The effects of isoprene emitted from urban green spaces on isoprene concentrations in urban Beijing are twofold. On the one hand, it improves the ability of the air quality model to reproduce the magnitude of isoprene concentrations. On the other hand, the diurnal cycle of isoprene concentrations better matches the observations. Nevertheless, whether differences in isoprene temporal variations between urban and rural areas are robustly applicable to other regions deserves more thorough investigation in future studies. Nevertheless, the ozone enhancement due to addition of the isoprene emissions from urban green spaces may robustly help to adjust the commonly seen underestimates in the simulated ozone concentrations particularly during high ozone pollution events over megacities (e.g., Sun et al. (2021), Guo et al. (2019), Wang et al. (2019), Li et al. (2013) and Tie et al. (2009)).

This study reveals the vital role of isoprene emissions from urban landscapes in modulating ozone formation. Previously, nine urban tree species in Denver has been examined to reveal that the selection of trees with low BVOC emission rates may be equivalent to the reduction in VOC emissions from a large number of cars (Curtis et al., 2014). Similarly, urban trees with low BVOC emission rates are likely to be essential in reducing the ozone forming potential (Calfapietra et al., 2013). Ozone has become an increasing concern in China despite the reduction in anthropogenic emissions; thus, the role of biogenic emissions must be seriously considered. In addition to BVOCs, urban landscapes and ecosystems may also lead to elevated emissions of biogenic reactive nitrogen species, such as HONO, NOx and NH_3 (Cheng et al., 2016; Oswald et al., 2013; Su et al., 2011; Su et al., 2020; Zheng et al., 2020), which may influence urban atmospheric chemistry and pollution in a similar manner.

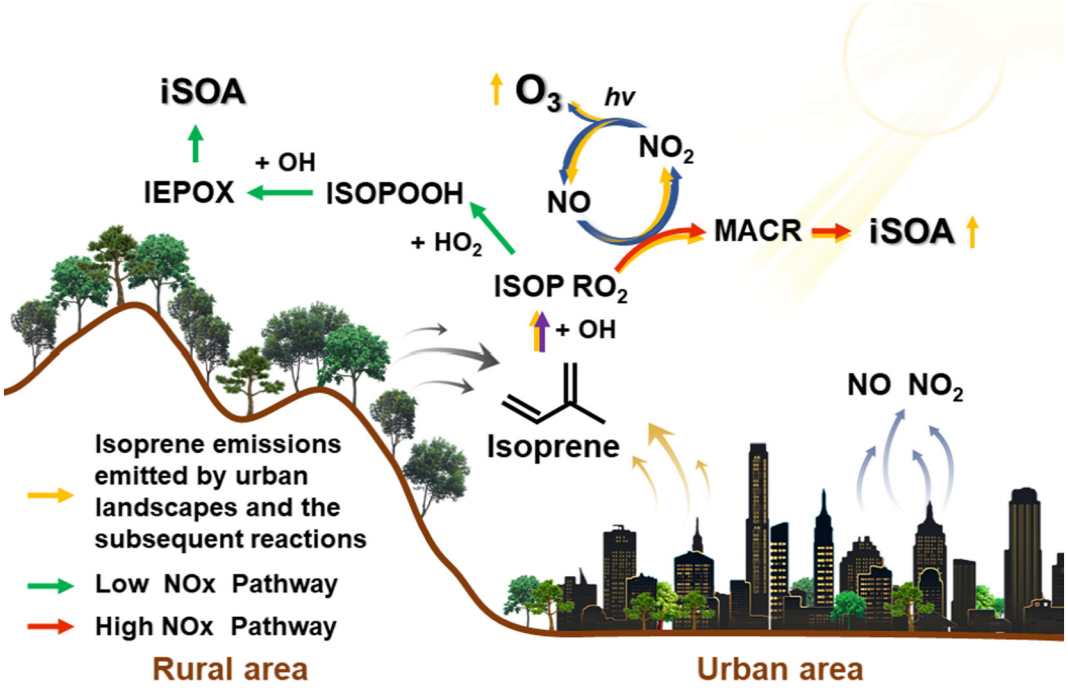

Fig. 6. A schematic diagram of the impact of isoprene emissions on ozone and SOA formation. The arrows in green and red represent the low and high NOx pathways by which isoprene yields SOA, respectively. The arrows in orange indicate isoprene emissions from the urban green spaces and subsequent impact on ozone and SOA, while the pathways of isoprene from other sources (e.g., non-urban area) are delineated by arrows in colors except orange. (For interpretation of the references to colour in this figure legend, the reader is referred to the web version of this article.)

Biogenic emission induced SOA contributes on average of 16% to the total SOA in Beijing. Moreover, the effect of isoprene emissions on SOA is closely associated with the abundance of NOx emissions. In megacities such as Beijing, which normally has high NOx emissions, the addition of isoprene emissions from urban landscapes yields an overall 36% increase in high NOx iSOA. Although the iSOA from the low NOx pathway is dominantly formed from non-urban or rural BVOC emissions, the transport might yield an even higher urban iSOA concentrations than those formed through the high NOx pathway. Considering the decreasing trend of NOx emissions in the future, the numerical sensitivities in this study reveal that low NOx iSOA resulting from urban BVOC emissions may display a sizable fractional increase. Therefore, further elucidation of BSOA, particularly the effect of urban BVOCs, will likely be helpful in comprehensively understanding its impact on urban aerosols and air pollution. Meanwhile, considering the positive role of trees in serving as carbon sink, helping to adjust the temperature and humidity and beautifying the environment of the urban areas (Gunawardena et al., 2017; Huang et al., 2011; Shashua-Bar et al., 2010), it is thus encouraged to expand the greening of cities concomitant with careful selection of the trees characterized of relatively low biogenic emissions rate as suggested in Ma et al. (2019).

Data availability

The data used in this study is available upon request to the corresponding author.

CRediT authorship contribution statement

Yang Gao: Conceptualization, Methodology, Formal analysis, Writing – original draft. **Mingchen Ma:** Visualization, Formal analysis. **Feifan Yan:** Formal analysis. **Hang Su:** Writing – review & editing. **Shuxiao Wang:** Validation, Formal analysis. **Hong Liao:** Validation, Writing – review & editing. **Bin Zhao:** Validation, Formal analysis, Writing – review & editing. **Xuemei Wang:** Writing – review & editing. **Yele Sun:** Writing – review & editing. **James R. Hopkins:** Validation. **Qi Chen:** Validation, Writing – review & editing. **Pingqing Fu:** Writing – review & editing. **Alastair C. Lewis:** Validation. **Qionghui Qiu:** Validation. **Xiaohong Yao:** Writing – review & editing. **Huiwang Gao:** Writing – review & editing.

Declaration of competing interest

The authors declare that they have no known competing financial interests or personal relationships that could have appeared to influence the work reported in this paper.

Acknowledgment

This research was supported by grants from the National Natural Science Foundation of China (91744208, 21625701), Fundamental Research Funds for the Central Universities (201941006), and Special Fund Project for Science and Technology Innovation Strategy of Guangdong Province (2019B121205004). The analysis was performed using the computing resources of the Center for High Performance Computing and System Simulation, Pilot National Laboratory for Marine Science and Technology (Qingdao).

Appendix A. Supplementary data

Supplementary data to this article can be found online at https://doi.org/10.1016/j.scitotenv.2021.152654.

References

Bell, M., Ellis, H., 2004. Sensitivity analysis of tropospheric ozone to modified biogenic emissions for the mid-Atlantic region. Atmos. Environ. 38, 1879–1889.

Bryant, D.J., Dixon, W.J., Hopkins, J.R., Dunmore, R.E., Pereira, K., Shaw, M., Squires, F.A., Bannan, T.J., Mehra, A., Worrall, S.D., et al., 2020. Strong anthropogenic control of secondary organic aerosol formation from isoprene in Beijing. Atmos. Chem. Phys. 20, 7531–7552.

Calfapietra, C., Fares, S., Manes, F., Morani, A., Sgrigna, G., Loreto, F., 2013. Role of biogenic volatile organic compounds (BVOC) emitted by urban trees on ozone concentration in cities: a review. Environ. Pollut. 183, 71–80.

Chen, F., Dudhia, J., 2001. Coupling an advanced land surface-hydrology model with the Penn State-NCAR MM5 modeling system. Part I: model implementation and sensitivity. Mon. Weather Rev. 129, 569–585.

Cheng, Y.F., Zheng, G.J., Wei, C., Mu, Q., Zheng, B., Wang, Z.B., Gao, M., Zhang, Q., He, K.B., Carmichael, G., et al., 2016. Reactive nitrogen chemistry in aerosol water as a source of sulfate during haze events in China. Sci. Adv. 2, 11.

Curtis, A.J., Helmig, D., Baroch, C., Daly, R., Davis, S., 2014. Biogenic volatile organic compound emissions from nine tree species used in an urban tree-planting program. Atmos. Environ. 95, 634–643.

Derognat, C., Beekmann, M., Baeumle, M., Martin, D., Schmidt, H., 2003. Effect of biogenic volatile organic compound emissions on tropospheric chemistry during the atmospheric pollution over the Paris area (ESQUIF) campaign in the ile-de-France region. J. Geophys. Res.-Atmos. 108, D17.

Ding, X., He, Q.F., Shen, R.Q., Yu, Q.Q., Wang, X.M., 2014. Spatial distributions of secondary organic aerosols from isoprene, monoterpenes, beta-caryophyllene, and aromatics over China during summer. J. Geophys. Res.-Atmos. 119, 11877–11891.

Ehn, M., Thornton, J.A., Kleist, E., Sipila, M., Junninen, H., Pullinen, I., Springer, M., Rubach, F., Tillmann, R., Lee, B., et al., 2014. A large source of low-volatility secondary organic aerosol. Nature 506, 476–479.

Emmons, L.K., Walters, S., Hess, P.G., Lamarque, J.F., Pfister, G.G., Fillmore, D., Granier, C., Guenther, A., Kinnison, D., Laepple, T., et al., 2010. Description and evaluation of the model for ozone and related chemical tracers, version 4 (MOZART-4). Geosci. Model Dev. 3, 43–67.

Farina, S.C., Adams, P.J., Pandis, S.N., 2010. Modeling global secondary organic aerosol formation and processing with the volatility basis set: implications for anthropogenic secondary organic aerosol. J. Geophys. Res.-Atmos. 115, D09202.

Friedl, M.A., Sulla-Menashe, D., Tan, B., Schneider, A., Ramankutty, N., Sibley, A., Huang, X.M., 2010. MODIS collection 5 global land cover: algorithm refinements and characterization of new datasets. Remote Sens. Environ. 114, 168–182.

Gao, Y., Shan, H.Y., Zhang, S.Q., Sheng, L.F., Li, J.P., Zhang, J.X., Ma, M.C., Meng, H., Luo, K., Gao, H.W., et al., 2020. Characteristics and sources of PM2.5 with focus on two severe pollution events in a coastal city of QingdaoChina. Chemosphere 247, 8.

Gao, Y., Yan, F.F., Ma, M.C., Ding, A.J., Liao, H., Wang, S.X., Wang, X.M., Zhao, B., Cai, W.J., Su, H., et al., 2021. Unveiling the dipole synergic effect of biogenic and anthropogenic emissions on ozone concentrations. Sci. Total Environ. 151722.

Grell, G.A., Freitas, S.R., 2014. A scale and aerosol aware stochastic convective parameterization for weather and air quality modeling. Atmos. Chem. Phys. 14, 5233–5250.

Guenther, A.B., Jiang, X., Heald, C.L., Sakulyanontvittaya, T., Duhl, T., Emmons, L.K., Wang, X., 2012. The model of emissions of gases and aerosols from nature version 2.1 (MEGAN2.1): an extended and updated framework for modeling biogenic emissions. Geosci. Model Dev. 5, 1471–1492.

Gunawardena, K.R., Wells, M.J., Kershaw, T., 2017. Utilising green and bluespace to mitigate urban heat island intensity. Sci. Total Environ. 584–585, 1040–1055.

Guo, H., Chen, K.Y., Wang, P.F., Hu, J.L., Ying, Q., Gao, A.F., Zhang, H.L., 2019. Simulation of summer ozone and its sensitivity to emission changes in China. Atmos. Pollut. Res. 10, 1543–1552.

Henrot, A.J., Stanelle, T., Schroder, S., Siegenthaler, C., Taraborrelli, D., Schultz, M.G., 2017. Implementation of the MEGAN (v2.1) biogenic emission model in the ECHAM6-HAMMOZ chemistry climate model. Geosci. Model Dev. 10, 903–926.

Hu, J.L., Wang, P., Ying, Q., Zhang, H.L., Chen, J.J., Ge, X.L., Li, X.H., Jiang, J.K., Wang, S.X., Zhang, J., et al., 2017. Modeling biogenic and anthropogenic secondary organic aerosol in China. Atmos. Chem. Phys. 17, 77–92.

Huang, G.L., Zhou, W.Q., Cadenasso, M.L., 2011. Is everyone hot in the city? Spatial pattern of land surface temperatures, land cover and neighborhood socioeconomic characteristics in BaltimoreMD. J. Environ. Manage. 92, 1753–1759.

Iacono, M.J., Delamere, J.S., Mlawer, E.J., Shephard, M.W., Clough, S.A., Collins, W.D., 2008. Radiative forcing by long-lived greenhouse gases: calculations with the AER radiative transfer models. J. Geophys. Res.-Atmos. 113, 8.

Janjic, Z.I., 1990. The step-mountain coordinate-physical package. Mon. Weather Rev. 118, 1429–1443.

Janjic, Z.I., 1994. The step-mountain eta coordinate model - further developments of the convection, viscous sublayer, and turbulence closure schemes. Mon. Weather Rev. 122, 927–945.

Jiang, J.H., Aksoyoglu, S., Ciarelli, G., Oikonomakis, E., El-Haddad, I., Canonaco, F., O'Dowd, C., Ovadnevaite, J., Minguillon, M.C., Baltensperger, U., et al., 2019. Effects of two different biogenic emission models on modelled ozone and aerosol concentrations in Europe. Atmos. Chem. Phys. 19, 3747–3768.

Li, Y., Lau, A.K.H., Fung, J.C.H., Ma, H., Tse, Y.Y., 2013. Systematic evaluation of ozone control policies using an ozone source apportionment method. Atmos. Environ. 76, 136–146.

Li, K., Jacob, D.J., Liao, H., Shen, L., Zhang, Q., Bates, K.H., 2019. Anthropogenic drivers of 2013–2017 trends in summer surface ozone in China. Proc. Natl. Acad. Sci. U. S. A. 116, 422–427.

Lin, Y.H., Zhang, H.F., Pye, H.O.T., Zhang, Z.F., Marth, W.J., Park, S., Arashiro, M., Cui, T.Q., Budisulistiorini, H., Sexton, K.G., et al., 2013. Epoxide as a precursor to secondary organic aerosol formation from isoprene photooxidation in the presence of nitrogen oxides. Proc. Natl. Acad. Sci. U. S. A. 110, 6718–6723.

Liu, Y., Li, L., An, J.Y., Huang, L., Yan, R.S., Huang, C., Wang, H.L., Wang, Q., Wang, M., Zhang, W., 2018. Estimation of biogenic VOC emissions and its impact on ozone formation over the Yangtze River Delta regionChina. Atmos. Environ. 186, 113–128.

Liu, S., Xing, J., Zhang, H.L., Ding, D., Zhang, F.F., Zhao, B., Sahu, S.K., Wang, S.X., 2019. Climate-driven trends of biogenic volatile organic compound emissions and their impacts on summertime ozone and secondary organic aerosol in China in the 2050s. Atmos. Environ. 218, 10.

Lu, X., Zhang, L., Chen, Y.F., Zhou, M., Zheng, B., Li, K., Liu, Y.M., Lin, J.T., Fu, T.M., Zhang, Q., 2019. Exploring 2016–2017 surface ozone pollution over China: source contributions and meteorological influences. Atmos. Chem. Phys. 19, 8339–8361.

Ma, M.C., Gao, Y., Wang, Y.H., Zhang, S.Q., Leung, L.R., Liu, C., Wang, S.X., Zhao, B., Chang, X., Su, H., et al., 2019. Substantial ozone enhancement over the North China plain from increased biogenic emissions due to heat waves and land cover in summer 2017. Atmos. Chem. Phys. 19, 12195–12207.

Ma, M.C., Gao, Y., Ding, A.J., Su, H., Liao, H., Wang, S.X., Wang, X.M., Zhao, B., Zhang, S.Q., Fu, P.Q., et al., 2021. The development and assessment of a high-resolution biogenic emission inventory from urban green space in China. Environ. Sci. Technol.

Mayrhofer, S., Teuber, M., Zimmer, I., Louis, S., Fischbach, R.J., Schnitzler, R.P., 2005. Diurnal and seasonal variation of isoprene biosynthesis-related genes in Grey poplar leaves. Plant Physiol. 139, 474–484.

McPherson, E.G., Simpson, J.R., Xiao, Q.F., Wu, C.X., 2011. Million trees Los Angeles canopy cover and benefit assessment. Landsc. Urban Plan. 99, 40–50.

Mellor, G.L., Yamada, T., 1982. Development of a turbulence closure model for geophysical fluid problems. Rev. Geophys. 20, 851–875.

Morani, A., Nowak, D.J., Hirabayashi, S., Calfapietra, C., 2011. How to select the best tree planting locations to enhance air pollution removal in the MillionTreesNYC initiative. Environ. Pollut. 159, 1040–1047.

Morcrette, J.J., Barker, H.W., Cole, J.N.S., Iacono, M.J., Pincus, R., 2008. Impact of a new radiation package, McRad, in the ECMWF integrated forecasting system. Mon. Weather Rev. 136, 4773–4798.

Morrison, H., Thompson, G., Tatarskii, V., 2009. Impact of cloud microphysics on the development of trailing stratiform precipitation in a simulated squall line: comparison of one- and two-moment schemes. Mon. Weather Rev. 137, 991–1007.

Nguyen, T.B., Bates, K.H., Crounse, J.D., Schwantes, R.H., Zhang, X., Kjaergaard, H.G., Surratt, J.D., Lin, P., Laskin, A., Seinfeld, J.H., et al., 2015. Mechanism of the hydroxyl radical oxidation of methacryloyl peroxynitrate (MPAN) and its pathway toward secondary organic aerosol formation in the atmosphere. Phys. Chem. Chem. Phys. 17, 17914–17926.

Oswald, R., Behrendt, T., Ermel, M., Wu, D., Su, H., Cheng, Y., Breuninger, C., Moravek, A., Mougin, E., Delon, C., et al., 2013. HONO emissions from soil bacteria as a major source of atmospheric reactive nitrogen. Science 341, 1233–1235.

Paulot, F., Crounse, J.D., Kjaergaard, H.G., Kurten, A., St Clair, J.M., Seinfeld, J.H., Wennberg, P.O., 2009. Unexpected epoxide formation in the gas-phase photooxidation of isoprene. Science 325, 730–733.

Qin, M.M., Wang, X.S., Hu, Y.T., Ding, X., Song, Y., Li, M.M., Vasilakos, P., Nenes, A., Russell, A.G., 2018. Simulating biogenic secondary organic aerosol during summertime in China. J. Geophys. Res.-Atmos. 123, 11100–11119.

Ren, Y., Qu, Z.L., Du, Y.Y., Xu, R.H., Ma, D.P., Yang, G.F., Shi, Y., Fan, X., Tani, A., Guo, P.P., et al., 2017. Air quality and health effects of biogenic volatile organic compounds emissions from urban green spaces and the mitigation strategies. Environ. Pollut. 230, 849–861.

Saha, S., Moorthi, S., Wu, X.R., Wang, J., Nadiga, S., Tripp, P., Behringer, D., Hou, Y.T., Chuang, H.Y., Iredell, M., et al., 2014. The NCEP climate forecast system version 2. J. Clim. 27, 2185–2208.

Shashua-Bar, L., Potchter, O., Bitan, A., Boltansky, D., Yaakov, Y., 2010. Microclimate modelling of street tree species effects within the varied urban morphology in the Mediterranean city of Tel AvivIsrael. Int. J. Climatol. 30, 44–57.

Su, H., Cheng, Y.F., Oswald, R., Behrendt, T., Trebs, I., Meixner, F.X., Andreae, M.O., Cheng, P., Zhang, Y., Poschl, U., 2011. Soil nitrite as a source of atmospheric HONO and OH radicals. Science 333, 1616–1618.

Su, H., Cheng, Y.F., Poschl, U., 2020. New multiphase chemical processes influencing atmospheric aerosols, air quality, and climate in the anthropocene. Acc. Chem. Res. 53, 2034–2043.

Sun, J., Shen, Z.X., Wang, R.N., Li, G.H., Zhang, Y., Zhang, B., He, K., Tang, Z.Y., Xu, H.M., Qu, L.L., et al., 2021. A comprehensive study on ozone pollution in a megacity in North China plain during summertime: observations, source attributions and ozone sensitivity. Environ. Int. 146, 14.

Tao, H.R., Xing, J., Pan, G.F., Pleim, J., Ran, L.M., Wang, S.X., Chang, X., Chen, F., Li, J., 2022. Impact of anthropogenic heat emissions on meteorological parameters and air quality in Beijing using a high-resolution model simulation. Front. Env. Sci. Eng. 16, 44.

Tie, X.X., Geng, F.H., Peng, L., Gao, W., Zhao, C.S., 2009. Measurement and modeling of O-3 variability in Shanghai, China: application of the WRF-chem model. Atmos. Environ. 43, 4289–4302.

Travis, K.R., Jacob, D.J., Fisher, J.A., Kim, P.S., Marais, E.A., Zhu, L., Yu, K., Miller, C.C., Yantosca, R.M., Sulprizio, M.P., et al., 2016. Why do models overestimate surface ozone in the Southeast United States? Atmos. Chem. Phys. 16, 13561–13577.

USEPA, 2007. Guidance on the Use of Models and Other Analyses for Demonstrating Attainment of Air Quality Goals for Ozone, PM2.5 and Regional Haze. EPA-454/B-07e002. USEPA.

Wang, R.N., Tie, X.X., Li, G.H., Zhao, S.Y., Long, X., Johansson, L., An, Z.S., 2019. Effect of ship emissions on O-3 in the Yangtze River Delta region of China: analysis of WRF-chem modeling. Sci. Total Environ. 683, 360–370.

Xu, W.Q., Xie, C.H., Karnezi, E., Zhang, Q., Wang, J.F., Pandis, S.N., Ge, X.L., Zhang, J.W., An, J.L., Wang, Q.Q., et al., 2019. Summertime aerosol volatility measurements in BeijingChina. Atmos. Chem. Phys. 19, 12.

Yan, F., Gao, Y., Ma, M., Liu, C., Ji, X., Zhao, F., Yao, X., Gao, H., 2021. Revealing the modulation of boundary conditions and governing processes on ozone formation over northern China in June 2017. Environ. Pollut. 272, 115999.

Zhang, P., Anderson, B., Barlow, M., 2004. Climate-related vegetation characteristics derived from moderate resolution imaging spectroradiometer (MODIS) leaf area index and normalized difference vegetation index. J. Geophys. Res.-Atmos. 109, 1–13.

Zheng, J.Y., Shao, M., Che, W.W., Zhang, L.J., Zhong, L.J., Zhang, Y.H., Streets, D., 2009. Speciated VOC emission inventory and spatial patterns of ozone formation potential in the Pearl River DeltaChina. Environ. Sci. Technol. 43, 8580–8586.

Zheng, G.J., Su, H., Wang, S.W., Andreae, M.O., Poschl, U., Cheng, Y.F., 2020. Multiphase buffer theory explains contrasts in atmospheric aerosol acidity. Science 369, 1374–1377.